Regular Article

PHYSICAL CHEMISTRY RESEARCH
Published by the
Iranian Chemical Society
www.physchemres.org
info@physchemres.org

***Phys. Chem. Res.**, Vol. 4, No. 2, 191-208, June 2016.*
DOI: 10.22036/pcr.2016.13575

Computational Study of the Mechanism, Reaction Rate and Thermochemistry of Atmospheric Oxidation of Methylamine with Singlet Oxygen

S. Valehi Reykandeh[a], M. Vahedpour[a,*], H. Douroudgari[a], S.A. Razavizadeh[b] and S. Asgharzadeh[a]

[a]*Department of Chemistry, University of Zanjan, P.O. Box: 45371-38791, Zanjan, Iran*
[b]*Department of Chemistry, Payame Noor University, P.O. Box: 19395-3697, Tehran, Iran*

(Received 24 November 2015, Accepted 17 February 2016)

The reaction of CH_3NH_2 with O_2 on the singlet potential energy surfaces (PES) was carried out using the B3LYP, CCSD(T) and G3B3 theoretical approaches along with 6-311++G(3df,3pd) basis set. The suggested mechanism for the title reaction consists of one pre-reactive complex. From the pre-reactive complex, nine types of products, $CH_2NH+H_2O_2$, $CH_3NH+OOH$, NH_2CHO+H_2O, CH_2NHO+H_2O, $NH_3+HCOOH$, $CH_2NH+H_2+O_2$, $HCHO+NH_2OH$, CH_2NH_2+HOO and CH_2NH+H_2OO are obtained. Six adducts are found to be thermodynamically stable with the negative value in Gibbs free energy and three products are not stable with positive value in Gibbs free energy at standard condition. NH_2CHO+H_2O and $NH_3+HCOOH$ with more free energy values are the thermodynamic products. CH_2NH and H_2O_2 are the major products for the title reaction. The rate constant for the major pathway is calculated in the temperature range of 300-1000 K at atmospheric pressure at the B3LYP//6-311++G(3df,3pd) level of computation.

Keywords: Methylamine, Reaction mechanism, Atmospheric oxidation

INTRODUCTION

Large amount of organic and inorganic compounds of both anthropogenic and biogenic sources are emitted into the atmosphere. The emission of such compounds may results in air pollution, acid deposition, long-rang transport of chemicals, depletion of the stratospheric ozone layer, and global climate modification, through a complex array of chemical and physical transformations [1].

Recent field measurements suggest that organic nitrogen species are among the major fraction of organic aerosol mass in atmosphere [2]. Amines are important class of organic nitrogen species, and are frequently detected in the form of aerosol, rain water, and fog water [3]. They are emitted into the atmosphere from a variety of sources including livestock, biomass burring, sewage treatment, industrial processes. The typical atmospheric concentration of alkyl amines is less in comparison with ammonia [4]. Methylamine is the simplest primary amine that has received considerable attention. This colorless gas is sold as a solution in methanol, ethanol, THF and water, or as the anhydrous gas in pressurized metal containers.

Methylamine production and its usage as an intermediate in the synthesis of pharmaceuticals, pesticides, solvents, explosives, surfactants, and photographic developers may result in its release to the environment through various waste streams.

In toxicology, the median lethal dose [5-7], LD50, of a toxin is the dose required to kill half the members of a tested population after specified test duration. LD50 figures are frequently used as a general indicator of a substance acute toxicity. LD50 is one way to measure the short-time poisoning potential (acute toxicity) of a compound. This quantity of CH_3NH_2 is 100-200 ppm. While for H_2O_2 and NH_2CHO, it is 1518 and 5000 ppm, respectively. Results show the toxicities of possible products are lower than the

*Corresponding author. E-mail: vahed@znu.ac.ir

reactants in comparison with using LD50 quantity.

Up to now, many experimental investigations on quantum chemical parameters and spectroscopic properties of CH_3NH_2 have been reported [8-10]. Ogryzlo *et al*. concentrated their effort on the electronic relaxation of the lowest singlet state of molecular oxygen to triplet stable state in the presence of methylamine. He shows that the rate constant of quenching of singlet oxygen is accelerated by adding amines [11]. Several theoretical studies have been also devoted to the reaction of CH_3NH_2 with OH [5], HNO_2 [12], HS [13], CO_2 [14] and so forth using the density functional theory or the *ab initio* methods.

In our previous work, we investigated the reaction mechanism of CH_3NH_2 with ozone on the singlet potential energy profile using computational method [15]. Our main objective in this article is to reveal the details of the reaction mechanism to explain the formation of possible products and provide further information about gaseous phase reaction of $CH_3NH_2 + O_2$ ($^1\Delta_g$) on the singlet potential energy surface. The calculated results from the present work are in good agreement with the available data in the literature.

COMPUTATIONAL DETAILS

All of the calculations reported in this paper are performed with the Gaussian 03 package [16]. The geometries of all species including the reactants, products, pre-reactive complex, possible intermediate and transition states located on the potential energy surfaces, PESs, are fully optimized at B3LYP/6-311++G(3df,3pd) [17] and G3B3 [18] level of theories. In this study, the largest basis set has been applied to obtain structures that are more reliable. For transition states, complexes and intermediates, we don't have any experimental data. So, two calculation methods have been used for the geometrical calculation. The calculations indicate that the geometrical parameters and barriers using these methods for the main reaction channels are in good agreement with each other. So, the selected methods for the calculation are good enough for the investigation of the reaction. Also, to obtain more accurate energies, single point calculations are performed for all species at the CCSD(T)//6-311++G(3df,3pd) level [19] based on B3LYP optimized structures. We report the T1 diagnostic values. In the case of the T1 diagnostic, the extent of multireference character in a given species is diagnosed by CCSD calculations, as described by Lee and Taylor [20]. The T1 diagnostic shows the used wave function to assess the reliability of these calculations with regard to a possible multireference character of the wave function at the corresponding stationary point. The T1 diagnostic values for all structures were calculated with CCSD(T) method.

At B3LYP and G3B3 levels, vibrational frequencies are computed for the verification of the nature of corresponding stationary points (minima or transition state). Any reactant, product and intermediate possess all real frequencies and any transition state has only one imaginary frequency. Zero point energies (ZPEs) plus thermodynamic contributions to the enthalpy and Gibbs free energies of reaction at T = 298.15 K and atmospheric pressure for the optimized structures were calculated at both mentioned methods. The application of the atoms in molecules, AIM, theory (Bader's theory) to understand the nature of the bonds in greater details is carried out [21]. This theory is based on the critical points (Cp) of the molecular electronic charge density, $\rho(r)$, and its gradient ($\nabla^2\rho(r)$). To verify the structures of all optimized species and their atomic connectivities, the topological analysis of atoms in molecules, AIM, theory [22] were carried out by means of the AIM2000 series of program [23].

Finally, connection between reactants, intermediates, transition states and products were confirmed by intrinsic reaction coordinate (IRC) [24] analysis which has been used to describe minimum energy paths from transition state structures to the corresponding minima at the B3LYP level.

RESULTS AND DISCUSSION

All possible elementary reactions begin with the formation of a pre-reactive complex that is designated by C1. The optimized geometries involved in the $CH_3NH_2 + O_2$ ($^1\Delta_g$) reaction on the singlet PES at the B3LYP//6-311++G(3df,3pd) level are shown in Fig. 1 and their Cartesian coordinates are collected in the supporting information. To simplify our discussion, the energy of reactant $CH_3NH_2 + O_2$ ($^1\Delta_g$) is denoted as R to reference on the singlet PES. The relative energies of CH_3NH_2 with O_2

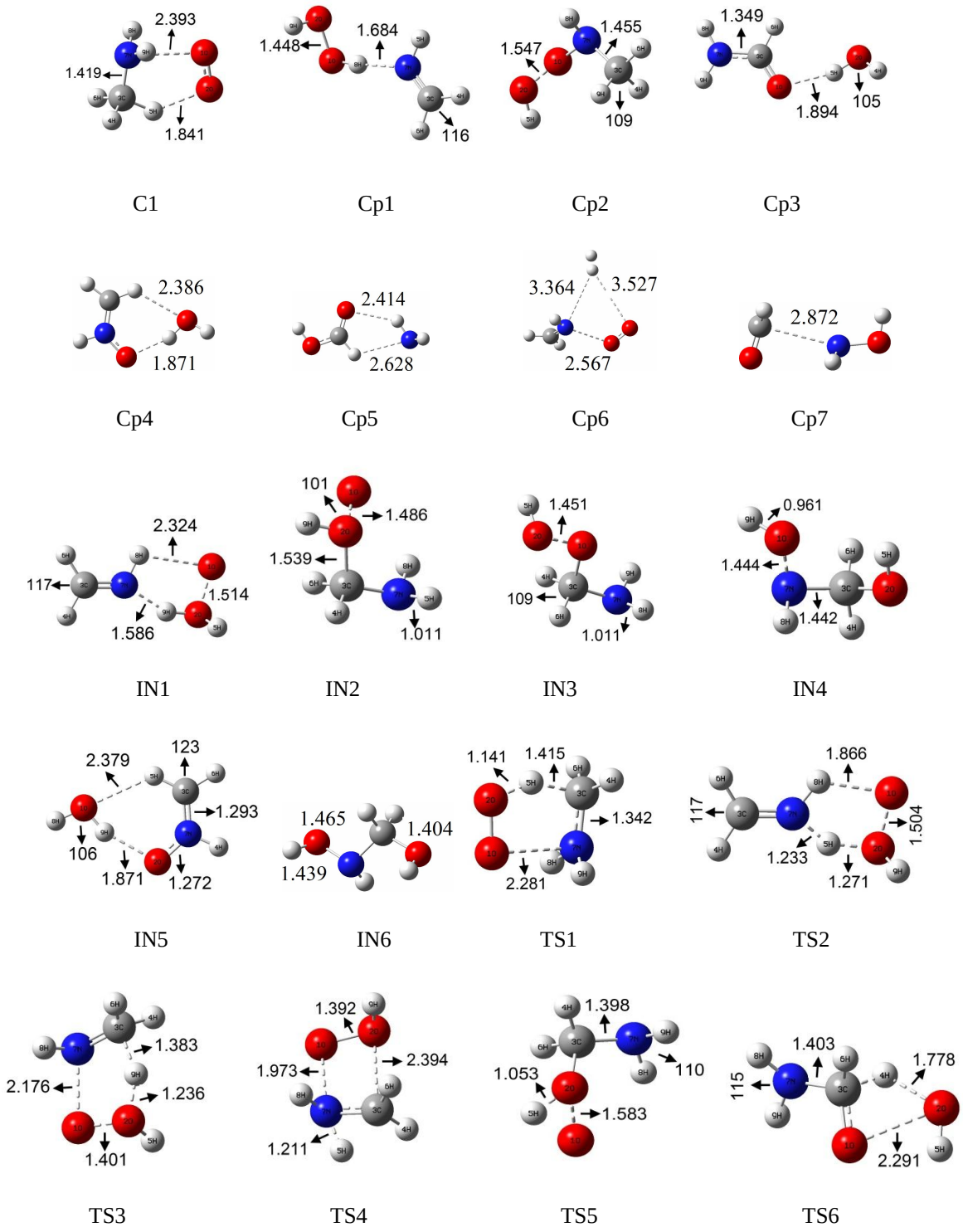

Fig. 1. Geometries of reactants, products, intermediates and transition states optimized at the B3LYP/6-311++G(3df,3pd) level (bond distances are in angstrom and angles are in degree).

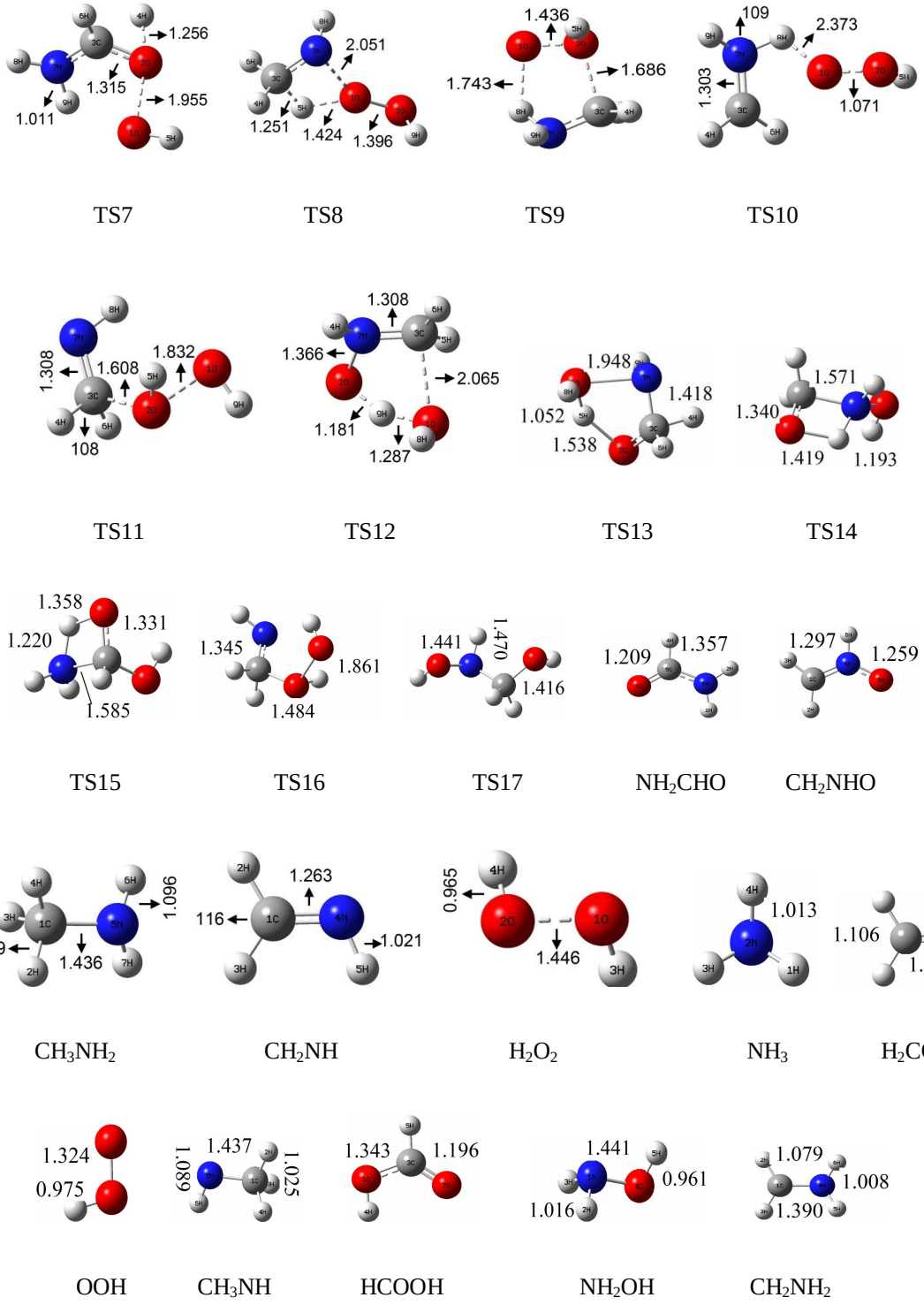

Fig. 1. Continued.

($^1\Delta_g$) reaction have been listed in Table 1 for the B3LYP, CCSD(T)//B3LYP//6-311++G(3df,3pd) and G3B3. T1 diagnostic in CCSD for confirming of selected of the computational method reliability and zero point energies in B3LYP for correction of thermodynamic variables are calculated. The calculated vibrational frequencies at the B3LYP level have been tabulated in supplementary information (Table 1S). For some stable molecules the obtained harmonic vibrational frequencies are compared with the corresponding available experimental values or with other calculated values. The comparison shows our results are in good agreement with them. Results show that

Table 1. Relative Energies and Zero Point Energies in kcal mol^{-1}, and T1 Diagnostic of the Reactants, Products and Intermediates in the $CH_3NH_2 + {}^1O_2$ ($^1\Delta_g$) Reaction at the B3LYP/6-311++G(3df,3pd), CCSD (T)/ 6-311++G(3df,3pd) and G3B3 Methods

Species	B3LYP	ZPE(B3LYP)	CCSD(T)	G3B3	ZPE(G3B3)	T1 diagnostic
$CH_3NH_2 + {}^1O_2$	0.00	42.36	0.00	0.00	41.07	-
C1	-6.50	43.29	-0.06	1.82	42.15	0.019
Cp1	-46.57	43.36	-43.46	-36.85	41.62	0.013
Cp2	-24.38	44.54	-21.72	-17.23	43.12	0.014
Cp3	-137.76	43.70	-135.10	-130.45	42.53	0.015
Cp4	-77.77	43.84	-74.50	-69.93	42.60	0.020
Cp5	-132.96	43.86	-131.44	-126.76	42.75	0.015
Cp6	22.70	34.77	31.36	16.81	34.24	0.014
Cp7	-68.28	42.96	-65.12	-62.95	41.61	0.014
IN1	-10.61	43.12	-6.03	-3.16	41.62	0.017
IN2	-17.44	45.73	-16.79	-9.27	44.21	0.018
IN3	-57.83	45.70	-58.30	-51.25	44.18	0.013
IN4	-77.26	46.40	-80.15	-70.88	44.81	0.012
IN5	-121.79	46.44	-126.65	-117.34	44.83	0.012
IN6	-77.31	46.34	-80.21	-71.33	44.62	0.012
TS1	-3.69	40.98	5.87	3.74	39.52	0.025
TS2	-10.39	40.54	-1.91	-4.68	38.85	0.018
TS3	15.68	41.03	25.41	22.75	39.58	0.030
TS4	37.29	41.28	44.79	41.99	39.79	0.038
TS5	-10.37	42.99	-8.70	-6.12	41.81	0.023

Table 1. Continued

TS6	7.14	40.72	3.67	-	-	0.024
TS7	-12.35	39.91	-1.38	-4.45	38.52	0.034
TS8	18.24	40.71	25.93	22.21	39.18	0.033
TS9	-16.02	44.14	-10.20	-7.18	42.68	0.026
TS10	-10.67	42.70	-0.88	1.23	40.52	0.035
TS11	41.75	37.27	57.97	-	-	0.021
TS12	-46.20	42.45	-39.93	-39.00	41.06	0.023
TS13	-29.71	41.80	-22.19	-18.19	40.56	0.035
TS14	-37.65	42.73	-34.93	-32.72	41.03	0.015
TS15	-88.78	43.14	-88.69	-85.32	41.53	0.014
TS16	11.97	41.55	4.18	56.57	40.51	0.077
TS17	-74.51	46.01	-76.64	-68.44	44.24	0.012
P1:$CH_2NH + H_2O_2$	-40.65	41.65	-34.95	-36.43	39.95	-
P2:$CH_3NH + OOH$	8.41	39.41	22.38	18.13	38.03	-
P3:$NH_2CHO + H_2O$	-133.58	41.79	-128.08	-128.90	40.01	-
P4:$CH_2NHO + H_2O$	-72.69	41.78	-65.88	-67.20	40.08	-
P5:$NH_3 + HCOOH$	-131.28	42.59	-127.14	-125.49	41.25	-
P6:$CH_2NH + H_2 + O_2$	23.49	33.63	33.17	15.01	32.50	-
P7:$H_2CO + NH_2OH$	-67.29	41.92	-61.88	-62.12	40.42	-
P8:$CH_2NH_2 + HO_2$	1.69	40.17	15.57	12.68	38.88	-
P9:$CH_2NH + H_2OO$	6.52	43.32	13.86	10.29	39.79	-

all of reactants, products, pre-reactive complexes and intermediates (INs) have real frequencies and each transition state has only one imaginary frequency. The standard thermodynamic functions (internal energies, enthalpies, Gibbs free energies and entropies of reaction) are tabulated in Table 2.

Topological analysis of atoms in molecules in electronic charge density and its Laplacian in bond and ring critical points, rcp, for all complexes are tabulated in Table 3. Also, three eigenvalues of the Hessian matrix (λ_i, i = 1, 2, 3) are collected in Table 3 that are used for discussion of atoms connectivity and origin of atomic bonds in molecules.

Finally, a schematic PES for $CH_3NH_2 + O_2$ ($^1\Delta_g$) reaction is plotted at B3LYP/6-311++G(3df,3pd) method in Fig. 2. The suggested mechanisms due to a complex reaction are as follows:

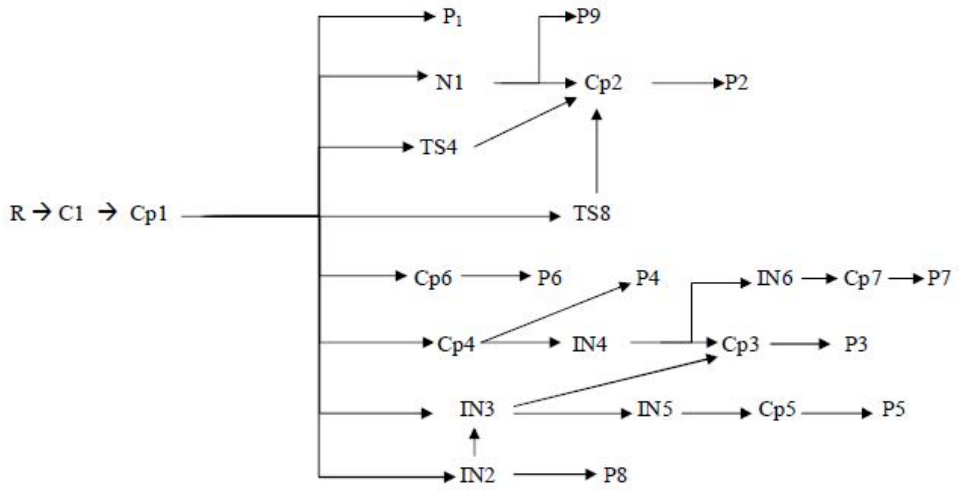

Scheme 1. The mechanism of the HSO + HS reaction

Table 2. The Thermodynamic Data for $CH_3NH_2 + {}^1O_2$ ($^1\Delta_g$) Reaction on the Singlet Potential Energy Surface at the B3LYP/6-311++G(3df,3pd) Method ΔE (kcal mol^{-1})

Step of reaction	ΔE°	ΔH°	ΔG°	$T\Delta S^\circ$
$CH_3NH_2 + {}^1O_2 \rightarrow CH_2NH + H_2O_2$	-40.45	-40.45	-42.1	1.65
$CH_3NH_2 + {}^1O_2 \rightarrow CH_3NH + HO_2$	8.72	8.72	6.08	2.64
$CH_3NH_2 + {}^1O_2 \rightarrow NH_2CHO + H_2O$	-133.1	-133.1	-134.17	1.07
$CH_3NH_2 + {}^1O_2 \rightarrow CH_2NHO + H_2O$	-72.5	-72.5	-73.03	0.53
$CH_3NH_2 + {}^1O_2 \rightarrow HCOOH + NH_3$	-131.13	-131.13	-132.08	0.94
$CH_3NH_2 + {}^1O_2 \rightarrow CH_3NHO + OH$	-13.37	-13.37	-14.47	1.1
$CH_3NH_2 + {}^1O_2 \rightarrow CH_2NH + H_2 + O_2$	24.63	25.23	16.93	8.3
$CH_3NH_2 + {}^1O_2 \rightarrow HCHO + NH_2OH$	-67.12	-67.12	-68.7	1.58
$CH_3NH_2 + {}^1O_2 \rightarrow CH_2NH_2 + HO_2$	2.02	2.02	2.52	-0.50
$CH_3NH_2 + {}^1O_2 \rightarrow CH_2NH + H_2OO$	4.8	4.8	3.23	1.57

In consequence of the reaction mechanism, we have found nine products. As shown in Scheme 1, all of the products are formed after crossing through unique stationary point Cp1 with different pathways. Also, the first product, P1, can be acquired of the reactants after passing one transition state. Details of the reaction mechanism on the singlet potential energy surfaces have been discussed in the next sections.

Reactants and Pre-reactive Complex

In spite of numerous attempts, just one pre-reactive cyclic complex (C1) is found on the singlet potential energy

Table 3. Topological Analysis of Molecules in some Species at the B3LYP/6-311++G(3df,3pd) Level, Values are in Atomic Units

Species	Bond	λ_1	λ_2	λ_3	ρ (r)	$\nabla^2\rho$ (r)
C1	N-O	-0.0346	-0.0241	0.1713	0.0316	0.112
	H-O	-0.0511	-0.0497	0.2175	0.0365	0.1166
	rcp	-0.0151	0.0292	0.0711	0.0164	0.0852
Cp1	N-H	-0.0598	-0.0579	0.1974	0.0368	0.0797
	C-H	-0.8331	-0.8212	0.5501	0.2936	-1.1041
	O=O	-0.6776	-0.6582	1.3035	0.2833	-0.0322
	O-H	-1.9437	-1.8731	0.9573	0.3575	-2.8595
Cp2	C-H	-0.7979	-0.7738	0.5267	0.2880	-1.0451
	N-H	-1.3691	-1.2916	0.8844	0.3547	-1.7763
	O-O	-0.6869	-0.6709	1.3657	0.2850	0.0079
Cp3	C-N	-0.8052	-0.7015	0.4241	0.3345	-1.0827
	N-H	-1.3780	-1.3136	0.8026	0.3507	-1.8891
	O-H	-0.0428	-0.0418	0.1763	0.0286	0.0916
Cp4	N-O	-1.1166	-1.0321	1.3951	0.4434	0.7536
	O-H	-0.0482	-0.0465	0.1887	0.0313	0.0940
	C-H	-0.8654	-0.8374	0.5641	0.2967	-1.1387
	rcp	-0.0067	0.0104	0.0326	0.0078	0.0363
Cp5	O-H	-0.0102	-0.0087	0.0536	0.0102	0.0347
	N-H	-0.0076	-0.0053	0.0408	0.0086	0.0279
	C-O	-1.2915	-1.1530	1.9608	0.4399	-0.4837
	rcp	-0.0061	0.0061	0.0338	0.0073	0.0337
Cp6	O-H	-0.0006	-0.0004	0.0045	0.0008	0.0034
	N-H	-0.0012	-0.0010	0.0077	0.0017	0.0054
	O-O					
	N-O	-0.4147	-0.0952	-0.9050	0.0188	0.0756
	rcp	-0.0005	0.0007	0.0032	0.0007	0.0034
Cp7	C-O	-1.2401	-1.1477	2.0798	0.4324	-0.3080
	C-N	-0.0072	-0.0064	0.0489	0.01070	0.0352
	N-O	-0.0110	-0.0007	-0.6576	0.2910	-0.3273
	O-H	-0.0029	-0.0255	-1.9454	0.3846	-3.0253
IN1	N-H	-0.1445	-0.1436	0.3480	0.0709	0.0599
	O1-H8	-0.0147	-0.0042	0.0803	0.0157	0.0615
	O2-H5	-1.5557	-1.5401	0.8219	0.3020	-2.2740
	rcp	-0.0142	0.0047	0.0775	0.0156	0.0679

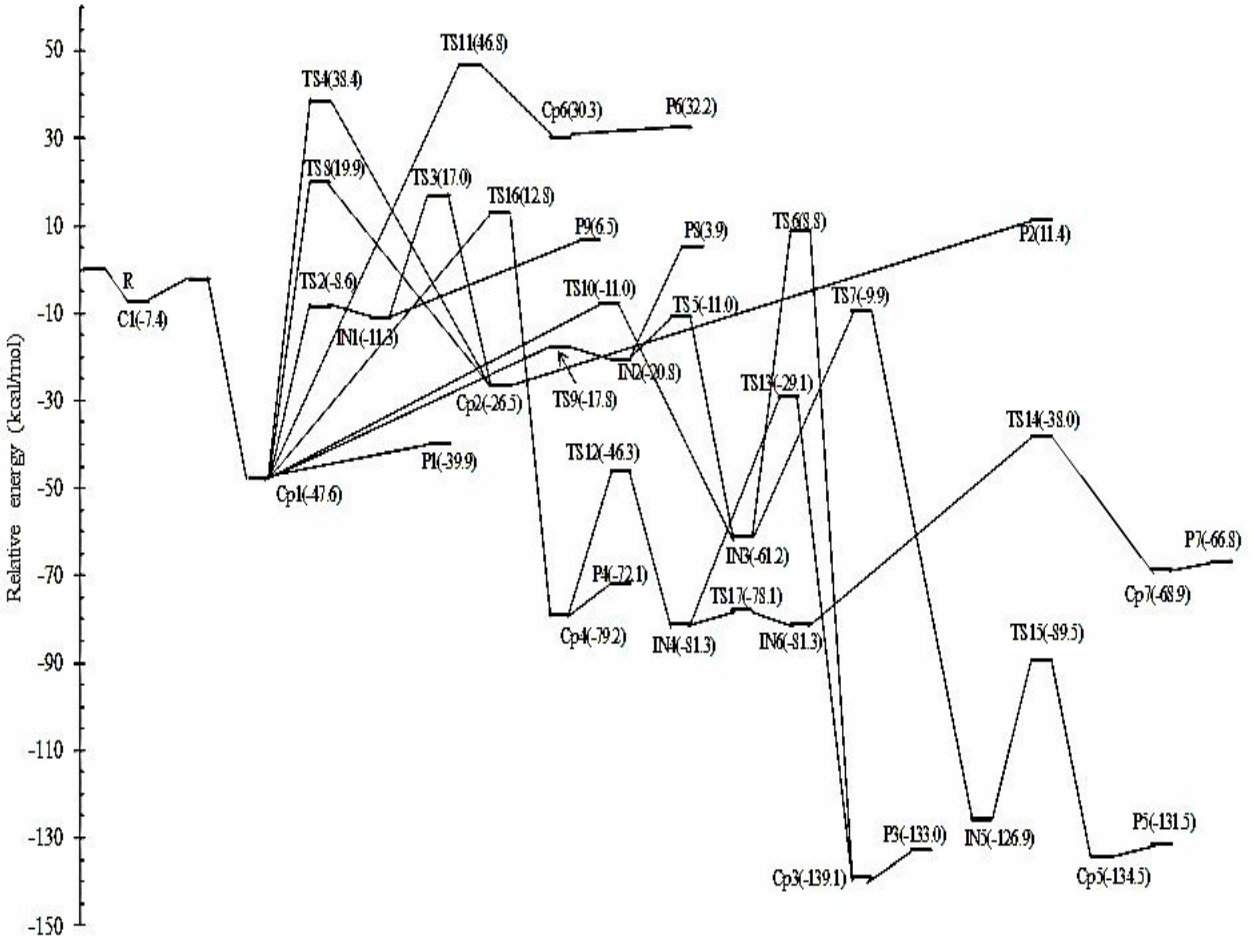

Fig. 2. Singlet potential energy profiles of the CH_3NH_2 + $^1O_2$ ($^1\Delta_g$) reaction at the B3LYP/6-311++G(3df,3pd) level.

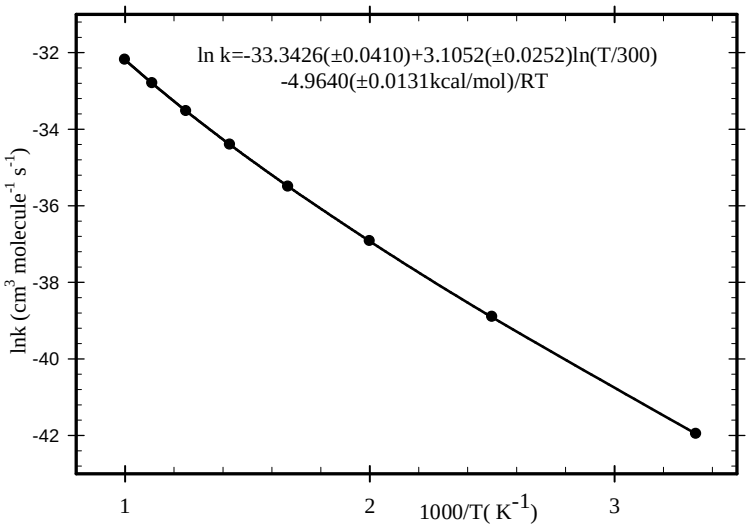

Fig. 3. Arrhenius plots for the path P_1 rate constant of the CH_3NH_2 + $^1O_2$ ($^1\Delta_g$) reaction at the B3LYP/6-311++G(3df,3pd) method.

surface. It is formed when nitrogen atom and one hydrogen atom of methyl group of CH_3NH_2 approaches into molecular oxygen from two tails without entrancing any energy barrier. Two newly intermolecular weak bonds in cyclic structure from two sides of molecular oxygen can cause low relative stability for C1 specie.

The newly formed H-O bond lengths in C1 are about 2.393 and 1.841 Å, respectively. It is 0.1 kcal mol^{-1} more stable than the original reactants at the CCSD (T) level. The complex formation between the original reactants is confirmed by atoms in molecules (AIM) topological analysis of wave function. This analysis reveals the presence of bond critical points (bcp) located between N-O and O-H bonds with density of the wave function, $\rho(r_{bcp})$ = 0.0314 and 0.0364 e $bohr^{-3}$ and the Laplacian of electronic density at critical point, $\nabla^2\rho(r_{bcp})$ = 0.1120 and 0.1162 e $bohr^{-5}$, respectively. These values show van der Waals origin for the new interactions.

Our calculations led to the identification of a complex mechanism for the reaction between methylamine and molecular oxygen on the singlet potential energy surfaces, which are summarized in Fig. 2.

Formation Pathway of P_1 ($CH_2NH + H_2O_2$)

For product P_1 ($CH_2NH+H_2O_2$), there is one possible path as follows:

Path P_1: R → C1 → TS1 → Cp1 → P_1 (R1)

In path P_1, at the first step, the initial pre-reactive complex, C1, is formed. C1 has a five-membered ring structure. Its ring structure is confirmed through AIM results with 0.0164 au in electronic charge density at ring critical point. Then, C1 transform into Cp1 *via* TS1 with the energy barrier of 5.3 kcal mol^{-1} at B3LYP/6-311++G(3df,3pd) level. Transition state TS1 has a five-membered ring structure with 0.0243 au in electronic charge density at ring critical point. It is 2.3 kcal mol^{-1} stable than the original reactants. The imaginary frequency of TS1 is 612 cm^{-1} at the B3LYP method. This structure is formed when the hydrogen atom of methyl group of CH_3NH_2 is transferred into oxygen molecule and simultaneously one of hydrogen atoms of NH_2 group shifts to molecular oxygen. The ring structure of TS1 collapses with the breaking of C-5H bond, and Cp1 is formed with a hydrogen bond between 8H and 7N atoms with the electronic charge density at bcp, $\rho(r_{bcp})$ = 0.0367 au and, $\nabla^2\rho(r)$ = 0.0795 a.u., in its Laplacian. Cp1 can be converted to the final product P_1 ($CH_2NH+H_2O_2$) through 8H-7N bond rupture without any energy barrier. The reaction thermodynamic parameters indicate that P_1 formation channel is exothermic in gas phase with -40.5 kcal mol^{-1} in the enthalpy of reaction.

The producing of P_1 pathway requires only one transition state with low level of energy in comparison with other pathways of transition states. Therefore, it can be considered as a kinetic path for the reaction and its product is defined as a kinetic product. In the rate constant section, the rate constant for the kinetic pathway of reaction using RRKM and TST theories are calculated and discussed.

Formation Pathway of P_2 ($CH_3NH + OOH$)

For product P_2 ($CH_3NH+OOH$), there are two possible pathways as follows:

Path P_2 (1): R → C1 → TS1 → Cp1 → TS8 → Cp2 → P_2 (R2)

Path P_2 (2): R → C1 → TS1 → Cp1 → TS4 → Cp2 → P_2 (R3)

Path P_2 (3): R → C1 → TS1 → Cp1 → TS2 → IN1 →TS3 → Cp2 → P_2 (R4)

In reaction path R2, the formation of Cp1 is similar to path P_1. Cp1 can be converted to Cp2 *via* TS8 with the energy barrier of 67.5 kcal mol^{-1} at the B3LYP/6-311++G(3df,3pd) method. The imaginary frequency of TS8 is 866 cm^{-1} in the reaction coordinate. TS8 has a four-membered ring structure with 0.0474 au in electronic charge density at the ring center and it is 19.9 kcal mol^{-1} unstable than the original reactants. TS8 are formed when a hydrogen atom from amine group of CH_3NH_2 molecule is transferred to the tail oxygen atom of molecular oxygen and at the same time O-O bond of molecular oxygen is weakening from 1.396 Å in TS8 to 1.547 Å in Cp2. TS8 undergoes 5H-1O bond rupture and is transformed into Cp_2 with disappearing of four-membered ring structure. Cp2 is a covalent bond between CH_3NH and OOH molecules with a negative low value in the Laplacian

of electronic charge density at critical point. Cp2 can be directly decomposed to CH_3NH+OOH products through N-O bond rupture without any transition state. The product CH_3NH+OOH is 37.9 kcal mol^{-1} above Cp2 that is related to N-O bond energy in Cp2 and 11.4 kcal mol^{-1} higher than the original reactants. Path P_2 (2), R3, to form Cp1 is the same as path P_2 (1). After that, Cp1 is transformed to Cp2 after passing TS4. TS4 energy is 18.473 kcal mol^{-1} higher than TS8. So, we expect this transformation is carried out by TS8.

In path P_2 (2), the formation of Cp1 is similar to that in path P_1. In this path, Cp1 can be converted to IN1 *via* TS2 with the energy barrier of 39.0 kcal mol^{-1} with formation of five-membered ring structure in TS2. Then, the ring structure rearranges to another five-membered structure in IN1. Electronic charge density at ring critical point of IN1 is 0.0156 a.u. compared to 0.0266 a.u. for TS2 which reflects the weakening of ring structure is in IN1. TS2 imaginary frequency along the reaction coordinate is 856 cm^{-1}.

The energy of intermediate IN1 is 36.2 kcal mol^{-1} higher than Cp1 and can be converted to CP2 through a five-membered ring transition state TS3 with collapsing of ring structure. The ring structure is confirmed for TS3 by using AIM analysis with 0.0269 a.u. in electronic charge density at ring critical point. In this process, O-O and O-9H bonds are ruptured and N-O bond is formed that can collapse the ring structure. The energy barrier for the IN1 → Cp2 conversion is 28.4 kcal mol^{-1} and imaginary frequency is 1122 cm^{-1}. The topological analysis for Cp2 reveals that for 1O-2O bond in this structure, electronic charge density of bcp is ρ(bcp) = 0.2194 a.u. and $\nabla^2\rho$ = 0.2018 a.u. which confirm strong van der Waals interaction. Also, for 3C-N bond in Cp2, electronic charge density of bcp is ρ(bcp) = 0.2714 a.u. and $\nabla^2\rho$ = -0.7495 au which confirm its covalent nature and reveal that the 3C-N bond length in Cp2 is 1.455 $\acute{A}$, 0.035 Å longer than corresponding bond in C1. Finally, Cp2 can be decomposed to CH_3NH and OOH products by N-O bond rupture without any transition state.

The formation of final adducts, CH_3NH and OOH, from original reactant is an endothermic and nonspontaneous process in the gas phase at atmospheric condition (see Table 2).

Formation Pathways of P_3 ($NH_2CHO + H_2O$)

For product P_3 ($NH_2CHO + H_2O$), there are two possible pathways as follows:

Path P_3 (1): R → C1→ TS1 → Cp1→ TS10 → IN3→ TS6 → Cp3 → P_3 (R5)

Path P_3 (2): R → C1 → TS1 → Cp1→ TS9 → IN2→ TS5 → IN3→ TS6 → Cp3 → P_3 (R6)

Path P_3(3): R → C1→ TS1 → Cp1→ TS16 → Cp4 → TS12 → IN4 → TS13 → Cp3 → P_3 (R7)

In these pathways, the formation of Cp1 is similar to that in path P_1. In path P_3 (1), R5 reaction, Cp1 *via* TS10 is transformed into IN3. The energy barrier for this conversion and imaginary frequency of TS10 are 36.6 kcal mol^{-1} and 310 cm^{-1}, respectively. Cp1 transformation to IN3 is similar s-trans to s-*cis* isomerization around H8-O1 bond and at the same time HO_2 groups shift from hydrogen atom to carbon atom. The energy of intermediate IN3 is 13.6 kcal mol^{-1} lower than that for the Cp1 and it can be transformed to Cp3 which undergoes 3C-4H and 1O-2O bonds rupture and 5H-1O bond formation via a four-membered ring transition state TS6. Electronic charge density at ring critical point of TS6 is 0.0343 au. The energy barrier for IN3→Cp3 transformation is 70.0 kcal mol^{-1} and the imaginary frequency of TS6 is 1417 cm^{-1} in the formation of four-membered ring structure.

AIM analysis reveals the presence of bcp in Cp3 located between 1O and 5H with electronic charge density of, ρ (r_{bcp}) = 0.0286 a.u. and the Laplacian of electronic charge density, $\nabla^2\rho(r_{bcp})$ = 0.0916 a.u. which confirm van dar Waals interaction. Product complex Cp3 is 135.1 kcal mol^{-1} more stable than the original reactants and it can be decomposed to final products, NH_2CHO and H_2O, with breaking of 1O-5H bond without entrancing into any transition state.

In path P_3 (2), Cp1 *via* TS9 with the energy barrier of 29.8 kcal mol^{-1} and imaginary frequency of 304 cm^{-1} transform into IN2. This transformation is explained by s-trans to s-*cis* isomerization and at the same time HO_2 groups shift from hydrogen atom to carbon atom using formation of a five-membered ring structure in TS9. AIM analysis

confirms TS9 ring structure with 0.0271 a.u. in electronic charge density at ring critical point. TS9 is transformed into IN2 by rupturing of H8-O1 bond and ring structure is disappeared. Intermediate IN2 is 20.8 kcal mol^{-1} more stable than the original reactants and can be transformed into IN3 *via* TS5. The energy barrier and imaginary frequency of TS5 for this conversion are 9.8 kcal mol^{-1} and 1325 cm^{-1}, respectively. IN2 undergoes IN3 after hydrogen migration from oxygen number one to other oxygen. The formation of Cp3 from IN3 and production of P_3 from Cp3 is similar to path P_3 (1) in R5 reaction.

AIM analyses reveal that intermediate IN2 has a covalent bond between 3C and 2O atoms with the electronic charge density at bcp, $\rho(bcp) = 0.197$ a.u. and, $\nabla^2\rho(r) = -0.304$ a.u., in its Laplacian. The formation of IN3 and then P_3 are similar to P_3 (2) pathway. P_3 is very stable with 133.0 kcal mol^{-1} energy lower than the original reactants. The R → P_3 conversion process is very exothermic and spontaneous with the standard enthalpy and Gibbs free energy of reaction, -133.1 and -134.2 kcal mol^{-1} in gas phase, respectively. P_3 is the most stable possible adduct of CH_3NH_2 plus molecular oxygen reaction. It is named as thermodynamic product.

In path P_3 (3), the formation of IN4 is similar to P_7 formation pathway that will be explained in section 3.8. IN4 *via* TS13 with the energy barrier of 52.2 kcal mol^{-1} and imaginary frequency of 782 cm^{-1} is transformed into Cp3. This transformation is explained by hydrogen shift from carbon atom to nitrogen atom and at the same time another hydrogen shift from O2 to O1 atoms and formation of water molecule fragment in Cp3. Then, it can be decomposed to final products, NH_2CHO and H_2O, with breaking of 1O-5H bond needless to energy barrier.

Formation Pathways of P_4 ($CH_2NHO + H_2O$)

For product P_4, there is one possible path as follows:

Path P_4: R → C1→ TS1 → Cp1→ TS16 → CP4 → P_4 (R8)

In formation pathway of P_4, R8 reaction, the formation of Cp1 is similar to previous pathways. In this path, Cp1 is transformed into Cp4 *via* TS16 with the energy barrier of 60.3 kcal mol^{-1}. The imaginary frequency of TS16 is 427 cm^{-1}. Intermediate Cp4 is 79.2 kcal mol^{-1} more stable than the original reactants. TS16 is formed when the two oxygen atoms are connected to each other using a van der Waals interaction. Cp4 is formed from TS16 when O-O van der Waals interaction is weakening and C-O covalent bond is stringing and at the same time hydrogen atom of this oxygen is transferred to OH group that is far from complex and form water molecule. Newly formed water molecule is a van der Waals complex with other side of molecule that is named Cp4. Product complex Cp4 has a six-membered ring structure with 0.0078 a.u. in electronic charge density at ring critical point. It undergoes rupture of the 2O-9H and 5H-1O bonds without any transition state to transform P_4. AIM analysis for Cp4 shows that product complex Cp4 has two van der Waals bonds, revealing the presence of bond Cps (bcps), located between 2O-9H with density of the wave function, $\rho(r_{bcp}) = 0.0310$ a.u. and the Laplacian of electronic charge density at Cp, $\nabla^2\rho(r) = 0.0940$ a.u. Electronic charge density at bond critical point between 1O and 5H bond is 0.0100 a.u. and its Laplacian is 0.0390 a.u.

Formation Pathways of P_5 (NH_3 + HCOOH)

For product P_4 ($NH_2CH(OH)_2$), there are two possible pathways as follows:

Path P_5 (1): R → C1 → TS1 → Cp1→ TS10 → IN3 → TS7 → IN5 → TS15→ Cp5→ P_5 (R9)

Path P_5 (2): R → C1 → TS1 →Cp1→TS9 → IN2 →TS5 → IN3 → TS7 → IN5 → TS15 → Cp5 → P (R10)

In R9 reaction, the formation of IN3 from Cp1 is similar to that of the R5 reaction. IN3 can be transformed into IN5 *via* TS7 with the energy barrier of 51.3 kcal mol^{-1}. The imaginary frequency of TS7 is 1267 cm^{-1} in the reaction coordinate. IN3 → IN5 transformation can be occurred by OH shift from oxygen number 2 to carbon atom of methylamine and species with two OH functional groups plus one NH_2 group is formed. In the next step, IN5 is converted into Cp5 *via* TS15 with the energy barrier of 36.3 kcal mol^{-1}. In this process one hydrogen atom from one of OH groups of IN5 is shifted to nitrogen atom of amine group. Then, an ammonia molecule is formed that has a van der Waals interaction with formic acid. The imaginary

frequency of the hydrogen transfer is 1653 cm^{-1} in the reaction coordinate. Finally the product complex, Cp5, is dissociated to NH_3 and HCOOH molecules as final adducts without passing any energy barrier.

In path P_5 (2), the formation of IN3 from IN2 is similar to path P_3 (2), R6, and the formation of P_5 from IN3 is similar to R9 reaction.

The formation of final adducts, ammonia and formic acid, from original reactants is exothermic with 131.1 kcal mol^{-1} heat releasing and spontaneous process with -132.1 kcal mol^{-1} in Gibbs free energy in the gas phase at atmospheric condition (see Table 2).

Formation Pathways of P_6 ($CH_2NH + H_2 + O_2$)

For product P_4 ($NH_2CH(OH)_2$), there is one possible pathway as follows:

Path P_6: R → C1 → TS1 → Cp1→ TS11 → Cp6 → P_6 (R11)

In path P_4, R11 reaction, the formation of Cp1 is similar to other pathways. Cp1 can be transformed into P_4 *via* TS11 with the energy barrier of 94.4 kcal mol^{-1}. The imaginary frequency of TS11 is 1090 cm^{-1} in the direction of two hydrogen atoms going away from the original molecule. One far from amine group and two far from OOH group of original molecule, Cp1, and at the same time these two hydrogens reach to each other and form hydrogen molecule. Then, the product van der Waals complex, Cp6, is dissociated to final adducts without entering to any energy barrier. The formation of final adduct, $CH_2NH + O_2 + H_2$, from the original reactants is an endothermic reaction with 25.2 kcal mol^{-1} in enthalpy of reaction and nonspontaneous process with +16.9 kcal mol^{-1} in Gibbs free energy in the gas phase at atmospheric condition (see Table 2). The entropy of the reaction increases more in comparison with other reaction products that is related to the formation of three molecules from two reactants that is related to the differences of translational entropy of the reaction.

Formation Pathways of P_7 (NH_2OH + HCHO)

For product P_7 (NH_2OH + HCHO), there is one possible pathway as follows:

Path P_7: R → C1 → TS1 → Cp1→ TS16 → Cp4 → TS12 → IN4 → TS17 → IN6 → TS14 → Cp7 → P_7 (R12)

In path P_7, R12 reaction, the formation of Cp4 is similar to R8 reaction. Product complex Cp4 can be transformed into IN4 *via* TS12. In this process, one hydrogen atom from water fragment of product complex migrates from oxygen atom of water to oxygen atom of CH_2NH_2O fragment with the formation of transition state (TS12). The energy barrier and imaginary frequency for this conversion are 33.0 kcal mol^{-1} and 1219 cm^{-1}, respectively. During this conversion the oxygen atoms of water fragment approaches to carbon atom of CH_2NH_2O fragment and forms IN4, simultaneously. In the next step, IN4 is converted into IN6 by s-*cis* to s-trans isomerization between N-C bond after entering TS17. The energy barrier and imaginary frequency of isomerization, TS17, are 3.1 kcal mol^{-1} and 148 cm^{-1}, respectively. After that, IN6 can be transformed into Cp7 *via* TS14 with the energy barrier of 43.3 kcal mol^{-1}. The imaginary frequency of TS14 is 1454 cm^{-1} in the direction at which hydrogen atom shifts from hydroxyl group bonded to carbon atom to nitrogen atom and forms one amine group. At the same time C-N bond is weakening and form Cp7 as product complex between formaldehyde fragment with hydroxyl amine fragment. Then, the product van der Waals complex, Cp7, is dissociated to the final adducts without entering to any transition state. The formation of final adduct, NH_2OH + HCHO, from original reactants is an exothermic reaction with -67.1 kcal mol^{-1} in enthalpy of reaction and spontaneous process with -68.7 kcal mol^{-1} in Gibbs free energy in standard condition (see Table 2).

Formation Pathways of P_8 (CH_2NH_2 + OOH) and P_9 ($CH_2NH + H_2OO$)

For product P_8 ($NH_2CHO + H_2O$), there is one possible pathway as mentioned for some pathways in producing IN2. This fragment can play a product complex role and C-O weak covalent bond breaks and P8 as final product with high level energy is produced. This dissociation needs to 24.7 kcal mol^{-1} energy and the production of P_8 is endothermic process with 2.0 kcal mol^{-1} standard enthalpy of reaction and spontaneous reaction with -0.5 kcal mol^{-1} in standard Gibbs free energy.

Product P_9 (CH_2NH + H_2OO) can be produced by breaking of two van der Waals bonds in IN1 ring. So, IN1 can play a product complex role (see Table 3 for AIM analysis) and adduct P_9 is obtained after breaking of O1-H8 and O2-H5 van der Waals bonds without passing of any transition state. This dissociation needs to 17.1 kcal mol^{-1} energy and the production of P_9 is endothermic process with 4.8 kcal mol^{-1} standard enthalpy of reaction and non-spontaneous reaction with 3.2 kcal mol^{-1} in standard Gibbs free energy.

The entropy of all reactions increases that is related to differences of internal degree of freedom except R9 reaction that translational degree of freedom has the main role.

Calculation of the Rate Constant

The rate constant is an important parameter. The rate constant for unimolecular reaction channel was calculated by RRKM (Rice-Ramsperger-Kassel-Marcus) theory. In RRKM theory [25], the thermal rate coefficient is obtained by integrating over E from E_0 to infinity of the Eq. (1) as follows:

$$k = \int_{E_0}^{\infty} \frac{k_2(E)\, dk_1(E)[M]}{k_{-1}[M] + k_2(E)} \tag{1}$$

where k_i, E_0, E and M are defined based on the Lindemann mechanism for the chemical reactions. The various terms of the rate expression are now evaluated using statistical mechanics. $k_2(E)$ is the microcanonical transition state theory rate constant and is given by:

$$k_2(E) = k_2(E_v, E_r) = \frac{1}{h} \frac{G\left(E_v + E_r\left[1 - \frac{l}{l^{\neq}}\right] - E_0\right)}{N(E_v)} \tag{2}$$

where $G(E^{\neq})$ is the sum of state for the active degree of freedom in the transition state, $N(E_v)$ is the density of states for the active degrees of freedom in the reactant, r and v refer to rotational and vibrational modes, respectively. In more detailed and accurate treatment of external rotational energy, the RRKM rate constant is written as a function of total energy E and angular momentum quantum number J;

$$k_2(E,J) = \frac{1}{h} \frac{1 G^{\neq}(E,J)}{N(E,J)} \tag{3}$$

where $G^{\neq}(E,J)$ is sum of states for the transition state, $N(E,J)$ is density of states for the energized molecule.

The RRKM rate constant for the overall thermal unimolecular reaction is found by inserting Eq. (3) into Eq. (1) and integrating over the Boltzmann distribution for E and J:

$$k_{unit} = \int_{E_0}^{\infty} dE \sum_{J=0}^{\infty} \frac{k_2(E,J) P(E,J)}{1 + k_2(E,J)/\omega} \tag{4}$$

where ω is the collision frequency and the distribution $P(E,J)$ is given by Eq. (5) as follows:

$$P(E,J) = \frac{(2J+1) N(E,J) \exp(-\frac{E}{k_B T})}{Q_r Q_v} \tag{5}$$

where $N(E,J)$ is the density of states for the reactant, and Q_r and Q_v are the rotational and vibrational partition functions of the reactants. Inserting Eq. (5) into Eq. (4) and replacing $K(E,J)$ with Eq. (3) and also using Laplace transform of $\Sigma(2J+1)\Sigma G^{\neq}(E,J,K)$ is the product of the external rotational and vibrational partition functions $Q_r^{\neq} Q_v^{\neq}$ for the transition state multiplied by $k_B T$, the rate constant at high pressure, k_{uni}^{∞} can be written as

$$k_{unt}^{\infty} = \frac{k_B T}{h} \frac{Q_r^{\neq} Q_v^{\neq} \exp\left(-\frac{E_0}{k_B T}\right)}{Q_r Q_v} \tag{6}$$

As it is seen, in the high pressure limit, RRKM theory reduces to transition state theory and the results of the two theories coincide.

The general expression for generalized transition-state theory (TST) is as follows [26-27]:

$$k(T)\, \Gamma \frac{k_B T}{h} \sigma \frac{Q^{\ddagger}}{Q_A Q_B} \exp\left(-\frac{V_{MEP}(s)}{k_B T}\right) \tag{7}$$

where Γ is the tunneling factor, σ is the reaction path degeneracy (the ratio of symmetry numbers from the rotational partition functions), the Q parameters are the product of translational, rotational, vibrational, and electronic partition for the transition state (numerator) and reactants (denominator), and s is the distance along the

reaction path from the saddle point. The reaction path is generally taken to be the minimum energy path (MEP) from the saddle point to the reactant and product geometries. V_{MEP} is the value of potential energy corrected for zero-point energy at the generalized transition-state theory. To show the influence of a possible tunneling process on the curvature of the Arrhenius plot at lower temperatures, calculations were carried out by including and excluding the tunneling factor.

The tunneling correction factor is defined as the quotient of the quantum mechanical rate to the classical rate. Although the tunneling process is a multidimensional phenomenon, this is treated as a one-dimensional process for simplicity. In this study, two methods were considered for the correction of possible tunneling effect. A simple expression, suggested by Shavitt for the tunneling correction, is:

$$Q_{\text{tunnel}} = 1 - \frac{1}{24}\left(\frac{h\nu^*}{k_B T}\right)^2 \left(1 + \frac{k_B T}{E_0}\right) \quad (8)$$

where ν* is the imaginary frequency of the activated complex at the top of the barrier, k_B and h are Boltzmann's and Plank's constants, and E_0 is the barrier height corrected for zero-point energy for the reaction.

On the singlet potential energy surfaces, the most suitable pathway is P_1. The rate constant has been calculated only for this suitable pathway by the RRKM and TST theories implemented in the Gaussian post processor, Gpop, program [28]. The Gpop program is standard software for the estimation of thermodynamic and rate constants for gas phase compounds and reactions. This program reads Gaussian output file containing a frequency job, extracts essential information such as density of state, microscopic rate coefficient and so on. It stores them in Gpop format file. The rate constant can be calculated after creating some master output files by software and solving a master equation based on our reaction channels.

The overall reaction pathway for P1 adducts is divided into three steps: two forward elementary reactions and one backward elementary reaction. The first step of forward reaction is bimolecular reaction ($CH_3NH_2 + O_2 \rightarrow$ C1). The rate constant for the mentioned step can be calculated using Eq. (7) for generalized transition-state theory. The second step and backward reaction are the unimolecular elementary reactions. The partial rate constants in general form for these steps are calculated by RRKM theory using Eq. (1). At high pressure, unimolecular rate constants are calculated by Eq. (6). Final rate constant at high pressure are obtained from product of forward reaction partial rates constant to dividing backward step, as: $k_{R\rightarrow CR}k_{CR\rightarrow Cp1}/k_{CR\rightarrow R}$

For path P_1 of the reaction of CH_3NH_2 with O_2 ($^1\Delta_g$), the calculated rate constant is detonated as *k*. Table 4 reveals that the values of *k* at the temperature range of 300-1000 K. Figure 4 shows the Arrhenius plot for the calculated title reaction rate constant. This figure shows that the rate constant for P1 pathway of title reaction has non-Arrhenius behavior at the mentioned temperature range. Therefore, the three-parameter expressions of the type $k = B(T/300)^m \exp(-E_b/RT)$ are used to show the temperature dependence of the calculated rate constant. The fitted rate constant into this equation for k_1 is in non-Arrhenius behavior as follows:

$$\ln k = -33.3426\,(\pm 0.0410) + \frac{3.1052\,(\pm 0.0252)\ln T}{300} - \frac{\frac{4.964\,(\pm 0.0131)\,kcal}{mol}}{RT} \quad (9)$$

To our knowledge, there is no direct experimental investigation to report rate constant of $CH_3NH_2 + O_2$ ($^1\Delta_g$) reaction at room temperature or any other condition. Therefore, we have suggestion the possible mechanism and rate constant value for the kinetic product of this reaction. The non-Arrhenius behavior might be related to the tunneling effect on two hydrogen shift on the reaction in the P1 pathway. The Arrhenius activation energy can be calculated by $E_a = E_b + mRT$. The calculated activation energy for the title reaction is 6.79 kcal mol^{-1} comparable with our previous work [16].

The comparison of our results with similar hydrogen abstraction reaction of methylamine by atmospheric hydroxyl radical from methyl and amine groups [7] show that form kinetic point of view the rate of oxidation of CH_3NH_2 with molecular singlet oxygen is smaller than that with other hydrogen abstraction by OH radical. This might be due to the activity of OH radical in comparison with singlet molecular oxygen. From the thermodynamic viewpoint, our suggested products are more stable than the

Table 4. Rate Constant of k Calculated at the Temperature Range of 300-1000 K at the B3LYP/6-311++G(3df,3pd) Method

Temperature (K)	*K* (cm^3 $molecule^{-1}$ s^{-1})
300	5.96×10^{-19}
400	1.27×10^{-17}
500	9.18×10^{-17}
600	3.81×10^{-16}
700	1.14×10^{-15}
800	2.74×10^{-15}
900	5.68×10^{-15}
1000	1.05×10^{-14}

products of CH_3NH_2 + OH hydrogen abstract reaction. So, we expect the oxidation of methylamine with $^1O_2$ to be more reliable than the CH_3NH_2 + OH reaction.

As we have seen in the Ogryzlo's paper [11] and our study, methylamine in the presence of molecular singlet oxygen can have the following two behavior: (a) quenching the singlet molecular oxygen to the triplet state; (b) reacting with singlet molecular oxygen. Comparison of our results with Ogryzlo's results at low temperatures (<400 K) ($k_{quenching} > k_{reaction}$) indicates that relaxation process is dominant. So, methylamine has quencher role. However, at temperature above 500 K chemical reaction process is a key part of the process ($k_{quenching} < k_{reaction}$). At temperatures in between, two processes are in competition with each other.

In the other work, the comparison of our calculated rate constant at 300 K, 5.96×10^{-19} cm^3 $molecule^{-1}$ S^{-1}, with the rate constant of $CH_3NH_2 + N_2O_3 + H_2O$ reaction [16] in the atmospheric condition, 1.296×10^{-19} cm^3 $molecule^{-1}$ S^{-1}, show the rate of CH_3NH_2 atmospheric degradation with singlet molecular oxygen and two nitric acid, $N_2O_3 + H_2O$, are comparable (our suggested reaction is 4.6 times faster).

Comparing the results of this work with our previous work [16] show that the reported heats of the reaction and Gibbs free energy in present work are more negative than those of the previous work. Therefore, the atmospheric oxidation of CH_3NH_2 using singlet molecular oxygen ($^1\Delta_g$) is more reliable than molecular ozone reported in our previous work. From kinetic point of view, the barrier height for kinetic pathway, TS1, is 6.0 kcal mol^{-1} compared with 15.6 and 21.2 kcal mol^{-1} for TS8 and TS9 of our previous work. So, the reaction of CH_3NH_2 with molecular singlet oxygen kinetically and thermodynamically is favorable. Also, all pathways in $CH_3NH_2 + O_2$ ($^1\Delta_g$) reaction have negative values of ΔG° and ΔH°, therefore all of them are exothermic and spontaneous.

CONCLUSIONS

From the present study, it is evident that:

1. In this work, details of the reaction mechanism of $CH_3NH_2 + O_2$ on the singlet PES have been characterized at the B3LYP, CCSD(T) and G3B3 level of computation in connection with the 6-311++G(3df,3pd) basis sets.
2. Nine kinds of products are obtained in this work. Six of them have enough thermodynamic stability. The results show that P_3 is the most stable product in compression with the others. Also, P_5 has more stability that is comparable with P_3.
3. From kinetic viewpoint, the P_1 adduct with one low level transition state is the main product. Also, its Gibbs free

energy is negative, so, we expect P_1 production is possible in the atmospheric condition.

4. Because of low energy levels of all transition states, the reaction of CH_3NH_2 + $^1O_2$ ($^1\Delta_g$) is an easy process at atmospheric conditions. Therefore, this reaction is produced so slightly atmospheric pollution.

5. Finally, the rate constant of the P_1 production channel is obtained using RRKM and TST theories at atmospheric pressure and temperature range from 300-1000 K in the gas phase. Non-Arrhenius behavior has been observed for the title reaction.

SUPPLEMENTARY DATA

Supplementary data associated with this article can be found in the online version at …..

ACKNOWLEDGEMENTS

We are highly grateful to University of Zanjan, for financial supporting of this work.

REFERENCS

[1] Yua, X.; Yia, B.; Wangb, X.; Chena, J. X.; Predicting reaction rate constants of ozone with organic compounds from radical structures. *Atoms. Environ.*, **2012**, *51*, 124-130, DOI: 10.1016/j.atmosenv. 2012.01.037.

[2] Liu, Y.; Han, C.; Liu, C.; Ma, J.; Ma, Q.; He, H., Differences in the reactivity of ammonium salts with methylamine. *Atoms. Chem. Phys.*, **2012**, *12*, 4855-4865, DOI: 10.5194/acp-12-4855-2012.

[3] Ge, X.; Wexler, A.; Clegg, S. L., Atmospheric amines-Part II. Thermodynamic properties and gas/ particle partitioning. *Atoms. Environ.*, **2011**, *45*, 561-577, DOI: 10.1016/j.atmosenv.2010.10.013.

[4] Ge, X.; Wexler, A.; Clegg, S. L., Atmospheric amines-Part I. A review, Atoms. Environ. *Atoms. Environ.*, **2011**, *45*, 524-546, DOI: 10.1016/ j.atmosenv.2010.10.012.

[5] Tian, W.; Wang, W.; Zhang, Y.; Wang, W., Direct dynamics study on the mechanism and the kinetics of the reaction of CH_3NH_2 with OH. *Int. J. Quantum Chem.*, **2009**, *109*, 1566, DOI: 10.1002/qua.22000.

[6] Canadian center for occupational health and safety (2005) chemical and material, LD50. http://www. ccochs.ca. Accessed 16 June 2005.

[7] Natural sourcing (2010) MSDS, Arnica flower total CO_2 extract. www.naturalsourcing.com. Accessed 25 may 2010.

[8] Alhambra, C.; Sanchez, M. L.; Corchado, J. C.; Gao, J.; Truhlar, D. G.; Quantum mechanical tunneling in methylamine dehydrogenase. *Chem. Phys. Lett.*, **2002**, *355*, 388-394, DOI: 10.1016/S0009-2614(02) 00057-X.

[9] Kaye, J. A.; Strobel, D. F., Formation and photochemistry of Methylamine in Jupiter's atmosphere. *ICARUS*, **1983**, *55*, 399-419, DOI: 10.1016/0019-1035(83)90111-2.

[10] Zhu, S.; Li, Q.; Dua, Y.; Yang, X.; Fan, J.; Dong, Z., Toxicity of derivatives from semicarbazide-sensitive amine oxidase-mediated deamination of methylamine against *Toxoplasma gondii* after infection of differentiated 3T3-L1 cells. *Toxical. In vitro*, **2010**, *24*, 809-814, DOI: 10.1016/j.tiv.2009.12.014.

[11] Ogryzlo, E. A.; Tang, C. W., Quenching of oxygen ($^1\Delta_g$) by amines. *J. Am. Chem. Soc.*, **1970**, *92*, 5034-5036, DOI: 10.1021/ja00720a005.

[12] Tiwary, S.; Mukherjee, A., Mechanism of the CH_3NH_2-HNO_2 reaction: *Ab initio* DFT/TST study. *J. Mol. Struct.: Theochem.*, **2009**, *909*, 57-65, DOI: 10.1016/j.theochem.2009.05.020 .

[13] Zhang, L.; Liu, H.; Tang, H.; Huang, T., Theoretical investigation on the reaction of HS+ with CH_3NH_2. *Chem. Pap.*, **2014**, *68*, 145-152, DOI: 10.1007/ s11178-006-0019-7.

[14] Kayi, H.; Kaiser, R.; Head, J., A computational study on the structures of methylamine-carbon dioxide-water clusters: evidence for the barrier free formation of the methylcarbamic acid zwitterion ($CH_3NH_2^+COO^-$) in interstellar water ices. *Phys. Chem. Chem. Phys.*, **2011**, *13*, 11083-11098, DOI: 10.1039/c0cp01962c.

[15] Valehi, S.; Vahedpour, M., Theoretical study on the mechanism of CH_3NH_2 and O_3 atmospheric reaction. *J. Chem. Sci.*, **2014**, *126*, 1173-1180, DOI: 10.1007/ s12039-014-0640-x.

[16] Frisch M. J. *et al*., *Gaussian 03* (Revision B 03). Gaussian, Inc., Pittsburgh, PA, **2003**.

[17] Becke, A. D., A new mixing of Hartree-Fock and local density-functional theories. *J. Chem. Phys*., **1993**, *98*, 1372-1377, DOI: 10.1063/1.464304.

[18] Curtiss, L. A.; Raghavachari, K.; Redfern, P. C.; Rassolov, V.; Pople, J. A., Gaussian-3 (G3) Theory for Molecules Containing First and Second-Row Atoms. *J. Chem. Phys.*, **1998**, *109*, 7764-7776, DOI: 10.1063/1.477422.

[19] J. Cizek, On the correlation problem in atomic and molecular systems. Calculation of wavefunction components in ursell-type expansion using quantum-field theoretical methods. *J. Chem. Phys.*, **1966**, *45*, 4256-4266.

[20] Lee, T. J.; Taylor, P. R., A Diagnostic for determining the quality of single reference electron correlation methods. *Int. J. Quantum Chem. Symp*., **1989**, *23*, 199, DOI: 10.1002/qua.560360824.

[21] Bader, R. F. W., A quantum theory of molecular structure and its applications. *Chem. Rev*., **1991**, *91*, 893-928, DOI: 10.1021/cr00005a013.

[22] Parr, R. G.; Yang, W., *Density-functional theory of atoms and molecules*, Oxford University Press, Oxford, **1989**.

[23] Biegler-Koing, F.; Schoenbohm, J., *AIM2000*, 2.0th edn. Buro fur Innovative software, Bielefeld, **2002**.

[24] Gonzalez, C.; Schlegel, H. B., Reaction path following in mass-weighted internal coordinates. *J. Phys. Chem*., **1990**, *94*, 5523-5527, DOI: 10.1021/ j100377a021.

[25] Forst, W., *Theory of Unimolecular Reactions*. Academic Press, New York, **1973**.

[26] Eyring, H., The activated complex in chemical reactions. *J. Chem. Phys*., **1935**, *3*, 107-115, DOI: 10.1021/cr60056a006.

[27] Ramazani, Sh., Direct-dynamics VTST study of hydrogen or deuterium abstraction and C-C bond formation or dissociation in the reactions of CH_3 + CH_4, CH_3 + CD_4, CH_3D + CD_3, CH_3CH_3 + H, and CH_3CD_3 + D. *J. Chem. Phys*., **2013**, *138*, 194305. DOI: 10.1063/1.4803862.

[28] A. Miyoshi, *Gaussian Post Processor* (GPOP). University of Tokyo, Tokyo, **2010**.

[29] Gray, A. P.; Lord, R. C., Rotation-vibration spectra of methylamine and its deuterium derivatives. *J. Chem. Phys.*, **1957**, *26*, 690, DOI: 10.1063/ 1.1743369.

[30] Shimanouchi, T., Tables of molecular vibrational frequencies. *Natl. Bureau. Stand.*, **1972**, 1.

[31] Malcom, W.; Chase, Jr.; NIST-JANAF Themochemical Tables, Fourth Edition. *J. Phys. Chem. Ref. Data*, Monogragh, **1998**, *9*, 1-1951.